Open Access Full Text Article

ORIGINAL RESEARCH

Electrospun Poly (Aspartic Acid)-Modified Zein Nanofibers for Promoting Bone Regeneration

Yun Liu [1],*
Ying-Ling Miao [2],*
Feng Qin[1]
Cen Cao[1]
Xiao-Lin Yu[1]
Yu-Han Wu[1]
Tian-Lu Wang[1]
Ruo-Gu Xu[1]
Liu Zhao[3]
Fan Wu[1]
Zheng-Chuan Zhang[1]
Jia-Min Yang[1]
Yang Yang[1]
Xin Xie[1]
Li-Ming Zhang[2]
Fei-Long Deng[1]

[1]Department of Oral Implantology, Guangdong Provincial Key Laboratory of Stomatology, Guanghua School of Stomatology, Sun Yat-Sen University, Guangzhou, Guangdong, People's Republic of China; [2]School of Materials Science and Engineering, Sun Yat-Sen University, Guangzhou, Guangdong, People's Republic of China; [3]School of Chemistry, Beihang University, Beijing, People's Republic of China

*These authors contributed equally to this work

Correspondence: Li-Ming Zhang
School of Materials Science and Engineering, Sun Yat-Sen University, No. 135, Xingang Xi Road, Guangzhou 510275, People's Republic of China
Tel +86 020-84112354
Email ceszhlm@mail.sysu.edu.cn

Fei-Long Deng
Department of Oral Implantology, Guangdong Provincial Key Laboratory of Stomatology, Guanghua School of Stomatology, Sun Yat-Sen University, No. 56, Lingyuan Xi Road, Guangzhou 510000, People's Republic of China
Tel +86 020-83863002
Email dengfl@mail.sysu.edu.cn

Background: Critical-sized bone defects raise great challenges. Zein is of interest for bone regeneration, but it has limited ability to stimulate cell proliferation. In this regard, a poly (aspartic acid) (PAsp)-zein hybrid is promising, as PAsp can promote rat bone marrow stromal cell (rBMSCs) proliferation and osteogenic differentiation. This research aimed to develop electrospun PAsp-modified zein nanofibers to realize critical-sized bone defects repair.

Methods: Three groups of PAsp-modified zein nanofibers were prepared, they were PAsp grafting percentages of 0% (zein), 5.32% (ZPAA-1), and 7.63% (ZPAA-2). Using rBMSCs as in vitro cell model and SD rats as in vivo animal model, fluorescence staining, SEM, CCK-8, ALP, ARS staining, μCT and histological analysis were performed to verify the biological and osteogenic activities for PAsp-modified zein nanofibers.

Results: As the Asp content increased from 0% to 7.63%, the water contact angle decreased from $129.8 \pm 2.3°$ to $105.5 \pm 2.5°$. SEM, fluorescence staining and CCK-8 assay showed that ZPAA-2 nanofibers had a superior effect on rBMSCs spreading and proliferation than did zein and ZPAA-1 nanofibers, ALP activity and ARS staining showed that ZPAA-2 can improve rBMSCs osteogenic differentiation. In vivo osteogenic activities was evaluated by μCT analysis, HE, Masson and immunohistochemical staining, indicating accelerated bone formation in ZPAA-2 SD rats after 4 and 8 weeks treatment, with a rank order of ZPAA-2 > ZPAA-1 > zein group. Moreover, the semiquantitative results of the Masson staining revealed that the maturity of the new bone was higher in the ZPAA-2 group than in the other groups.

Conclusion: Electrospun PAsp-modified zein can provide a suitable microenvironment for osteogenic differentiation of rBMSCs, as well as for bone regeneration; the optimal membrane appears to have a PAsp grafting percentage of 7.63%.

Keywords: electrospun, osteogenesis, poly (aspartic acid), zein

Introduction

Currently, autogenous bone grafting is the most common treatment for bone defects but repairing critical-sized bone defects remains a clinical challenge worldwide.[1,2] Bone tissue engineering (BTE) holds great promise to address this issue effectively, and scaffold biomaterials are essential for BTE. In recent decades, widespread efforts have been made to develop polymeric biomaterials. Unlike other biomaterials, the physical, chemical, and biological properties of polymers can be precisely regulated at the molecular level.[3] Although several polymers have been tried in medical applications, clinically, there are few successful examples. Synthetic polymers are limited in terms of their chemical composition, and most have shortcomings associated with biodegradability.[4] As an alternative to synthetic polymers, natural polymers provide many important benefits, including biocompatibility,

degradability, lower toxicity, and higher biological stability. Recently, protein-based biomaterials have become attractive because their macromolecular structures are similar to those of natural proteins in bone tissues. Among these proteins, plant proteins are more promising than animal proteins, as they are easier to obtain and have less immunogenic potential.

As a major storage protein of corn, zein has recently attracted attention in tissue engineering applications due to its perfect membrane-forming behavior, ability to preserve the functions of the natural extracellular matrix (ECM), inherent biocompatibility, excellent mechanical properties (flexibility, toughness, and compressibility), appropriate degradability, antioxidant activity, and resistance to microbial degradation.[4,5] However, the hydrophobic properties of zein and its ability to stimulate cell proliferation remain limited. Molecular engineering of polymers with bioactive molecules provides the means to stimulate cellular responses, inducing cell proliferation and differentiation at the molecular level.[3,6] Aspartic acid (Asp) has been reported to have specific beneficial effects on bone regeneration[7,8] by inducing rat bone marrow stromal cell (rBMSC) proliferation, osteogenic differentiation, and extracellular mineralization. These findings prompted us to fabricate poly (aspartic acid) (Asp)-modified zein, in which the Asp peptide is used to promote osteogenic differentiation. For example, several noncollagenous bone proteins, such as bone sialoprotein and osteopontin (OPN), have repeating Asp-rich sequences that can potentially serve as hydroxyapatite-binding sites; additionally, Asp has a high affinity for hydroxyapatite[9] and acts as an apatite nucleating agent, influencing further growth.

Biomolecule-polymer hybrids can be prepared via the simultaneous copolymerization of biomolecular and polymer units, or by conjugation of specific bioactive molecules onto polymer skeletons. Compared with conventional physical absorption, chemical bioconjugation is more versatile and controllable. However, identification of suitably mild conditions, as well as achieving high efficiency, remain major challenges. Click chemistry can be used to prepare biomolecule - polymer hybrids with well-defined properties. In this study, we prepared PAsp-modified zein using click chemistry.

As an ideal tool, nanofibrous scaffolding can be shaped to fill any anatomical defect.[10] Given the growing literature on the importance of the cellular microenvironment, bone tissue engineers are seeking to mimic the ECM,[11] which plays an important role in controlling cell behavior.[12,13] Electrospinning has emerged as a promising technique, as it can be used to create nanofibrous scaffolds that simulate the biophysical cues of native ECM.[11,14,15] This study aimed to develop such electrospun fibers to realize critical bone defect repair, and we hypothesized that electrospun PAsp-modified zein nanofibers can provide suitable microenvironment for bone regeneration. In the present research, we first prepared and characterized electrospun PAsp-modified zein and used rBMSCs as model cells for in vitro osteogenesis analysis. The electrospun PAsp-modified zein nanofibrous membranes were then implanted into critical-sized rat cranial bone defects to assess their ability to promote bone growth/repair (Figure 1).

Materials and Methods
Materials
Zein (Z3625), collagenase type I (COL-1), and pentobarbital sodium solution were purchased from Sigma Aldrich (St.
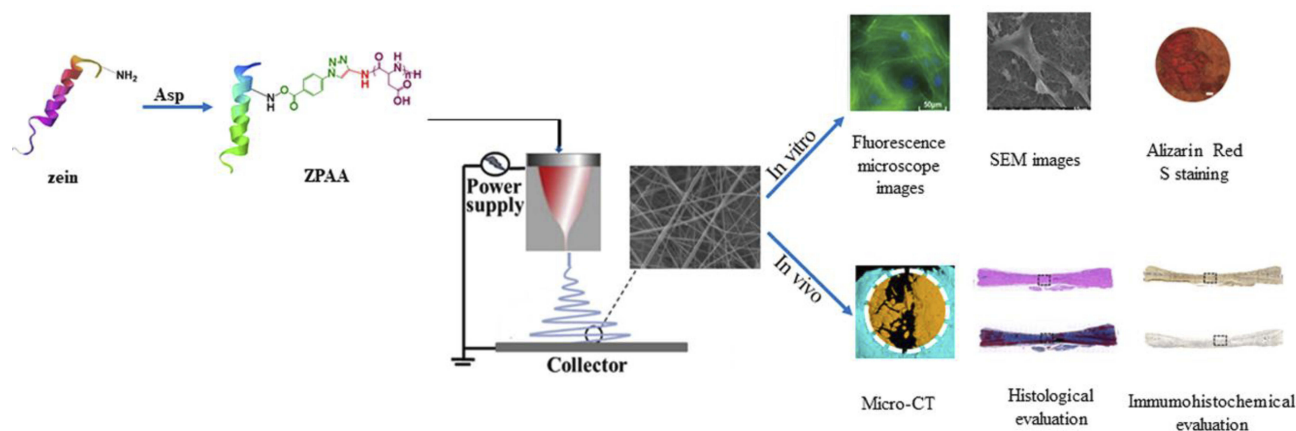
Figure 1 Schematic preparation of poly (*L*-aspartic acid)-modified zein and its potential application for bone defect regeneration.

Louis, MO, USA). L-Aspartic acid β-benzyl ester (98%), propargylamine (98%), trifluoroacetic acid (TFA, 99%) 1-ethyl-3-(3-dimethylaminopropyl)-carbodiimide (EDC) (98%), N-hydroxy-succinimide (NHS) (98%), 4-azidobenzoic acid (96%), and sodium ascorbate (99%) were sourced from Aladdin Chemical Company (Shanghai, People's Republic of China). Triphosgene (99.5%) was purchased from Xiya Reagent (Shandong, People's Republic of China). 1,1,1,3,3,3-Hexafluoro-2-propanol (HFIP, 99%) and hydrogen bromide (33 wt% in acetic acid) were purchased from the Energy Chemical Company (Shanghai, People's Republic of China). Tetrahydrofuran (THF, 99.5%) and dimethylformamide (DMF, 99.5%) were purchased from Sinopharm Chemical Reagent Corp (Shanghai, People's Republic of China). Dulbecco's modified Eagle's medium (DMEM) and antimycotic antibiotic solution were purchased from Gibco (Carlsbad, CA, USA), and fetal calf serum was purchased from Hyclone (Logan, UT, USA). The Cell Counting Kit-8 (CCK-8) was from Dojindo (Kumamoto, Japan). A bicinchoninic acid protein assay kit was purchased from Beyotime (Shanghai, People's Republic of China), and an alkaline phosphatase (ALP) assay kit was purchased from Jiancheng (Nanjing, People's Republic of China). Alizarin red S (ARS) was obtained from Sigma Chemical Company (Darmstadt, Germany). Phalloidin was purchased from AAT Bioquest (Sunnyvale, CA, USA), and 4′,6-diamidino-2-phenylindole (DAPI) was from Telenbiotech (Guangzhou, People's Republic of China). Three-day-old Sprague–Dawley (SD) rats were obtained from the Experimental Animal Center of Sun Yat-sen University (Guangzhou, People's Republic of China) and 9-week-old SD rats were purchased from the Experimental Animal Center of Guangzhou University of Chinese Medicine (Guangzhou, People's Republic of China).

Preparation of Zein/ZPAA-1/ZPAA-2 Nanofibrous Membranes and Characterization
The synthetic route of ZPAA is shown in Figure 2.

Preparation of L-Aspartic Acid β-Benzyl Ester N-Carboxyanhydride (BAA-NCA)
L-aspartic acid β-benzyl ester (10.00 g, 44.80 mmol) was suspended in 100 mL of anhydrous THF. Triphosgene (7.16 g, 24.13 mmol) was then added at 50°C under the protection of N_2. The reaction mixture was cooled to room temperature, and THF was removed by rotary evaporation. The residue was subsequently redissolved in 100 mL of ethyl acetate, and the solution was washed with cold saturated $NaHCO_3$ solution until no gas formed. After washing with cold deionized water three times, the organic

layer was dried over $MgSO_4$ and concentrated under vacuum. Finally, L-aspartic acid BAA-NCA was obtained as a white solid product (yield: 91%).

Preparation of Poly(Β-Benzyl-L-Aspartate) (Alkynyl-PBAA)
BAA-NCA (1.00 g, 4.02 mmol) was dissolved in 10 mL of anhydrous DMF. To prepare the PBAA-1/PBAA-2 solution, propargylamine (4.6 μL, 0.067 mmol, $[M]_0/[I]_0$=60; 3.1 μL, 0.045 mmol, $[M]_0/[I]_0$=90) was added under the protection of N_2, with stirring for 3 days. Diethyl ether was used to precipitate the product. Finally, the obtained white solid product was dried under vacuum (yield: 88%).

## Preparation of Poly (L-Aspartic Acid) (Alknyl-PAA)
Alkynyl-PBAA (5.00 g) was dissolved in 10 mL of TFA, and hydrogen bromide (3.0 mL, 33 wt% in acetic acid) was added dropwise at 0°C. After 2 h, the mixture was concentrated under vacuum to remove the solvents. The obtained solid product was subsequently washed thoroughly with deionized water and dried under vacuum (yield: 62%).

Preparation of Azidobenzoic Acid-Grafted Zein (Zein-N₃)
4-Azidobenzoic acid (0.10 g, 0.613 mmol) was dissolved in 20 mL of anhydrous dimethyl sulfoxide (DMSO). Then, EDC (0.06 g, 0.307 mmol) and NHS (0.04 g, 0.307 mmol) were added, with stirring for 2 h. Zein (0.50 g) was subsequently added. For fabricating azidobenzoic acid-grafted zein (zein-N_3), the reaction was performed for 3 days at room temperature; diethyl ether was used to precipitate the product. Finally, the obtained yellow solid product was dried under vacuum (yield: 91%).

Preparation and Characterization of Poly (L-Aspartic Acid)-Grafted Zein (ZPAA)
Zein-N_3 (0.10 g) was dissolved in 30 mL of DMSO. After adding Alknyl-PAA (0.04 g)/Asp-2 (0.08 g), $CuSO_4 \cdot 5H_2O$ (0.06 g, 0.240 mmol) and L-ascorbic acid sodium salt (NaAsc, 0.09 g, 0.454 mmol) were added under the protection of N_2. For preparing poly (L-aspartic acid)-grafted zein, the reaction was performed for 3 days at 50°C, and the mixture was dialyzed for 1 day. The solid product thus obtained was then washed with water and dried under vacuum (yield: 72%). The synthesis conditions of ZPAAs was summarized in Table 1. The synthesis of poly (L-aspartic acid)-grafted zein was then confirmed by proton nuclear magnetic resonance (^1H NMR) and Fourier
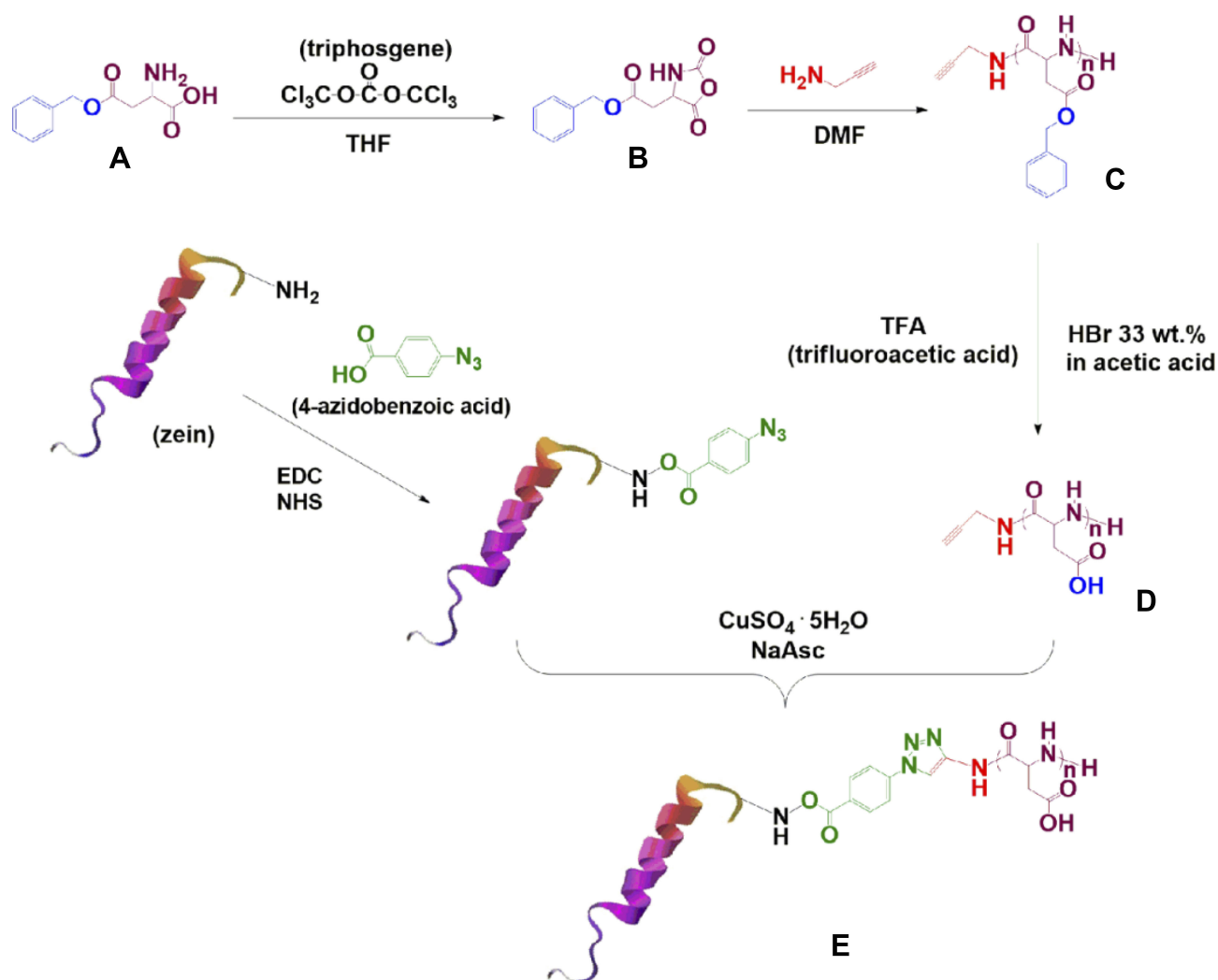
Figure 2 Synthesis of poly (L-aspartic acid)-grafted zein.

transform infrared (FTIR) spectroscopy. ^{1}H NMR spectra were recorded on an INOVA 500NB superconducting Fourier-transform NMR system (Varian, Palo Alto, CA, USA). FTIR spectra were obtained with a Nicolet 670 FTIR spectrometer (Thermo Nicolet, Madison, WI, USA).

Preparation and Characterization of Zein/ZPAA-1/ZPAA-2 Nanofibrous Membranes

Zein/ZPAA-1/ZPAA-2 (1.00 g) samples were dissolved in 5.0 mL of HFIP. To fabricate zein/ZPAA electrospun nanofibrous membranes, electrospinning was performed with typical

electrospinning parameters of 20-kV voltage and a flow rate of 0.008 mm/min. Electrospun membranes were sputter-coated with gold and visualized by scanning electron microscopy (SEM; JSM-6330F; JEOL, Ltd., Tokyo, Japan). The mean diameter of the nanofibers was calculated based on 300 random diameters. The contact angle of each nanofibrous membrane was measured using a Kruss DSA10-MK system (Kruss GmbH, Hamburg, Germany). To study biodegradability, the membranes were immersed in phosphate-buffered saline (PBS; pH 7.4, containing 10 mg/mL COL-1) for 7 days and then observed by SEM. Each sample was measured three times.

Mineralization of Zein/ZPAA-1/ZPAA-2 Nanofibrous Membranes

A 10 × SBF-solution was prepared as described in a previous publication.[16] Briefly, a stock solution was prepared according to Table S1 (pH 4.1) and NaHCO$_3$ was added to adjust the

Table 1 Synthesis Conditions of ZPAAs

Sample	BGA-NCA (g)	Zein (g)	DMF (mL)	Yield %
ZPBGA-1	0.50	5.00	20	86.2
ZPBGA-2	0.50	2.50	20	85.7

concentration of HCO_3^- to 10 mM. After cutting the membrane into a sample size of $10 \times 10 \times 0.05$ mm^3, zein, ZPAA-1, and ZPAA-2 nanofibrous membranes were immersed in aqueous acetic acid solution (0.001 mol/L) for 2 min, and then in $10 \times$ SBF solution for 2, 3, or 4 h. The mineralized nanofibrous membranes were rinsed thoroughly with deionized water three times and vacuum-dried before SEM evaluation.

Cell Seeding on Zein/ZPAA-1/ZPAA-2 Nanofibrous Membranes

The zein/ZPAA-1/ZPAA-2 nanofibrous membranes were cut into discs (diameter: 0.65 cm) and placed into 96-well plates. The zein nanofibrous membrane was used as the control group and the membrane-free plate as the blank group. The samples were subjected to ultraviolet (UV) radiation for 12 h and then incubated in DMEM complete culture medium consisting of 89% (v/v) DMEM, 10% (v/v) FCS and 1% (v/v) penicillin/streptomycin solution (P/S) for 30 min. rBMSCs were obtained from SD rat bone marrow, as described in a previous study,[17] and rBMSCs at passages 3–5 were implanted in the nanofibrous membranes.

Proliferation and Morphology of rBMSCs
Proliferation of rBMSCs

rBMSC proliferation was assayed using CCK-8 according to the manufacturer's instructions. In brief, rBMSCs were seeded onto the membranes at a density of 1×10^5 cells/mL and cultured in DMEM complete medium. The medium was changed every 2 days. At 1, 3, 5, 7 and 14 days after rBMSC seeding, 10 μL of CCK-8 was added to each well (n = 3), and the cells were incubated at 37°C with 5% CO_2 in the dark. Two hours later, the media were transferred to a 96-well plate to measure the optical density values at an optical wavelength of 450 nm using an enzyme-linked immunosorbent assay reader.

Morphologies of rBMSCs

SEM. BMSCs were seeded on the membranes at a density of 1×10^4 cells/mL and cultured in DMEM complete medium. The medium was changed every 2 days. After 1 day, 3 days, and 5 days of culture, rBMSCs on zein/ZPAA-1/ZPAA-2 nanofibrous membranes were rinsed with PBS three times and fixed in 2.5% glutaraldehyde solution for 1 h. After fixation, the samples were dehydrated with 100% ethanol solution. Thereafter, the samples were dried, coated with gold, and examined by SEM (Quanta 400F thermal field emission environmental SEM; FEI, Lyon, France).

Fluorescent staining of phalloidin and DAPI. The morphology of rBMSCs on zein/ZPAA-1/ZPAA-2 nanofibrous membranes was further observed by staining with DAPI (blue fluorescence) and phalloidin (green fluorescence), for cell nuclear and F-actin labeling, respectively. After culturing (1×10^4 cells/mL) for 1, 3, and 5 days, cell-seeded nanofibrous membranes were fixed in 3.7% formaldehyde solution for 5 min and permeabilized with 0.1% Triton X-100. Thereafter, the samples were stained with phalloidin and DAPI for 60 and 10 min, respectively. Then, the cells/membranes were examined using fluorescence inverted microscopy (Axio Observer A1; Carl Zeiss AG, Oberkochen, Germany).

Osteogenic Differentiation of rBMSCs

rBMSC osteogenic differentiation assays were performed using an ALP activity test and ARS staining. Briefly, rBMSCs were seeded on the membranes at a density of 1×10^5 cells/mL and incubated overnight in DMEM complete medium under standard culture conditions (5% CO_2 at 37°C). Twenty-four hours later, the medium was replaced by osteogenic medium (10 mM β-glycerophosphate, 10 nM dexamethasone, and 50 mg/mL ascorbic acid).

ALP activity. ALP activity was measured using an ALP activity assay kit. Briefly, after culturing for 7 and 14 days, ALP activity was measured following standard procedures.[18] Activity was normalized against the total protein content, which was measured using a bicinchoninic acid kit according to the manufacturer's instructions.

ARS staining. After culturing for 14 days, ARS staining was applied to determine the presence of calcium. Briefly, the nanofibrous membranes were washed with PBS and fixed with 4% formaldehyde solution for 15 min. The fixed cells were then stained with 2% Alizarin red (pH 4.2) for 5 min and rinsed with PBS three times. All membranes were assayed under a bright field microscope.

Surgical Procedures

To evaluate the osteogenic potential of different zein membranes, an in vivo SD rat (male, 9 weeks old, 250–300 g) critical-sized cranial bone defect model was used. The rats were purchased from the Experimental Animal Center of Guangzhou University of Chinese Medicine and were kept under specific-pathogen-free conditions of the Animal Center of Sun Yat-sen University, at 26°C with a 12-h light/dark cycle. The rats were provided with a standard pellet rodent diet and water. The experimental protocol complied with the UK Animals (Scientific Procedures) Act and the ARRIVE

guidelines. The animal experiments were approved by the Animal Care and Use Committee of Sun Yat-sen University (Permit Number: IACUC-DB-16-0315). The rats were anesthetized by injection of 0.1% pentobarbital sodium solution under aseptic conditions, and the cranium was exposed through a medial incision. Bilateral full-thickness circular defects (diameter: 6 mm; thickness: 1 mm) were then made by dental burs. Before being implanted into the defects, zein/ZPAA-1/ZPAA-2 nanofibrous membranes were cut into discs (diameter: 6 mm) and subjected to UV radiation for 12 h (Figure S1). In total, 24 defects (12 rats) were created in this study. The animals were divided into four groups (n = 3): the ZPAA-1, ZPAA-2, zein, and blank control (left untreated) groups. The rats were sacrificed after 4 and 8 weeks.

## Micro Computed-Tomography (Micro-CT) and Histological Analysis

Micro-CT analysis. After rats were euthanized, at 4 (n = 6) and 8 weeks (n = 6) postoperatively, bone samples were excised and fixed in 10% (v/v) neutral formalin for 24 h. Then, new bone was visualized and quantified using micro-CT (μCT50; Scanco Medical AG, Wangan-Bruttisellen, Switzerland). Three-dimensional (3-D) reconstructions of the images were then created using VG studio Max2.2 (Volume Graphics, Heidelberg, Germany). A series of parameters, including bone volume/tissue volume (BV/TV), bone surface/bone volume (BS/BV), trabecular thickness (Tb.Th), trabecular number (Tb.N), and trabecular bone space (Tb.Sp), was evaluated. Moreover, we modified the method of Spicer et al[19,20] and scored the bony union and bridging according to Table 2.

Histological and immunohistochemistry analysis. For histological analysis, the samples were made into paraffin sections, which were then processed for hematoxylin and eosin (H&E) and Masson's trichrome (MT) staining. For MT staining, semiquantitative detection of the red dyed areas was performed by Image Pro Plus 6.0 software. Moreover, for testing COL-1 and osteocalcin (OCN) expression, the paraffin sections were subjected to immunohistochemical staining. The stained sections were photographed digitally under a microscope.

Statistical Analysis

All quantitative data are presented as means ± standard deviation. One-way analysis of variance followed by Tukey's test was performed for statistical comparisons. A value of $p < 0.05$ was deemed statistically significant. All

**Table 2** Modified Scoring Guides for the Extent of Bony Union and Bridging

Bony Bridging Extent	Score	Models
No bone formation	0	
Few bony islands dispersed throughout the defect	I	
Bony bridging only at the defect margins	2	
Bony bridging over the partial length of the defect	3	
Bony bridging over the entire span of the defect at the longest point	4	
Bone almost filled the full defect	5	

data were analyzed using SPSS software (ver. 21.0; IBM Corporation, Armonk, NY, USA).

Results
Synthesis of ZPAA

The synthesis of ZPAA was confirmed by ^{1}H NMR and FTIR spectroscopy (Figure 2). ^{1}H NMR spectra of zein, zein-N_3, and ZPAA are shown in Figure 3A. Asp and zein shared a peak at 4.79 ppm (CH groups) and at 2.83 ppm (CH$_2$ groups).[21] However, the peak of ZPAA appearing at 7.53 ppm (triazole ring) confirmed the click reaction between alkynyl-Asp and zein-N_3. FTIR spectra of zein, zein-N_3, and ZPAA are shown in Figure 3B. The main peak of zein-N_3 appeared at 2124 cm^{-1} (azido group conjugation). For the spectrum of ZPAA, the main peak appeared at 1403 cm^{-1} (COOH group), whereas the typical azido group bond at 2124 cm^{-1} was detected, indicating the conjugation of Asp on zein and the success of the
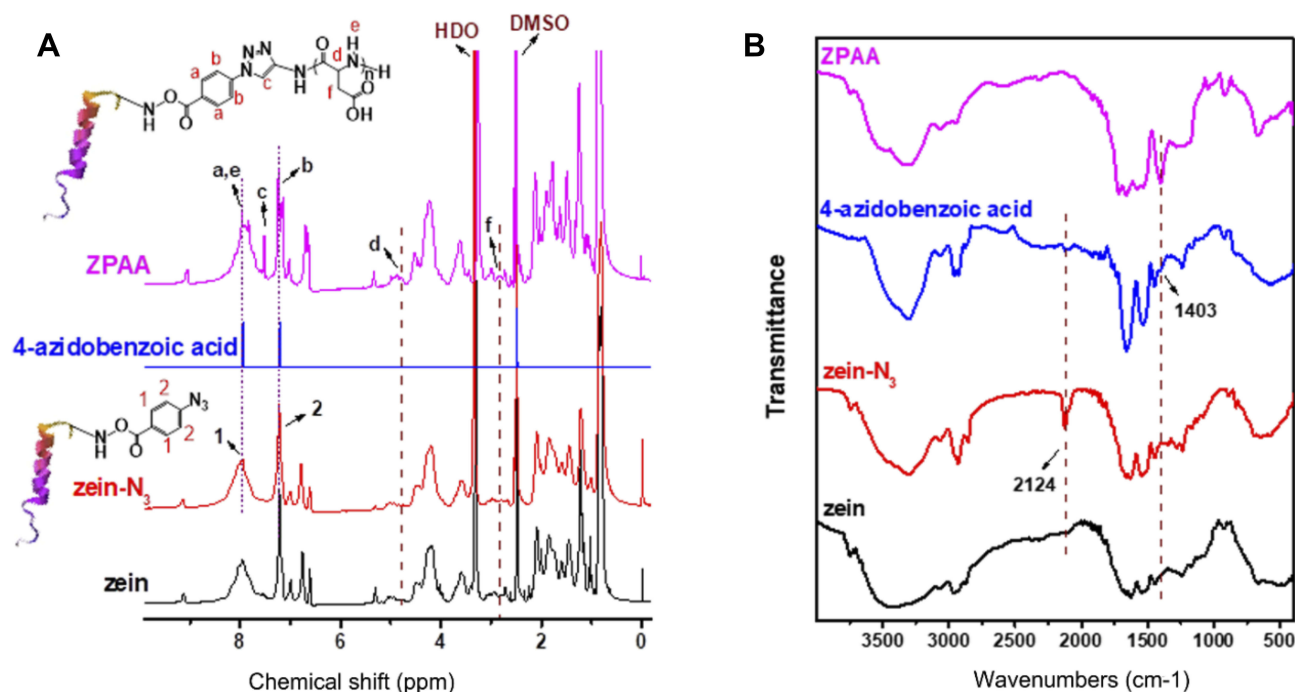
Figure 3 (A) Proton nuclear magnetic resonance and (B) Fourier transform infrared spectra of zein, zein-N3, 4-azidobenzoic acid, and poly (L-aspartic acid)-grafted zein.

click reaction, respectively.[22,23] The grafting percentages of ZPAA-1 and ZPAA-2 [grafting percentage = m(polymer)/m(zein) × 100%] were calculated to be 5.32% and 7.63%, based on element analysis.

Characterization of the Electrospun Membranes

An electrospinning technique was used to fabricate zein/ZPAA-1/ZPAA-2 nanofibrous membranes. SEM morphologies revealed successful generation of uniform fibrous structures for all electrospun membranes. All nanofibers showed highly porous networks. The diameters of the zein, ZPAA-1, and ZPAA-2 membranes were 87 nm, 148 nm and 215 nm, respectively. (Figure 4A). Furthermore, the water contact angles of zein, ZPAA-1, and ZPAA-2 membranes were 129.8 ± 2.3°, 113.6 ± 1.8°, and 105.5 ± 2.5°, respectively. As the Asp content increased from 0% to 7.63%, the water contact angle decreased from 129.8 ± 2.3° to 105.5 ± 2.5°. The results reveal that Asp chains improved the surface wettability of ZPAA membranes (Figure 4B). Moreover, in the biodegradability test (Figure S2A), holes and broken areas indicated that addition of Asp did not affect membrane biodegradation.

The in vitro bone bioactivities of zein/ZPAA-1/ ZPAA-2 nanofibrous membranes were analyzed in terms

of the apatite mineralization behavior in SBF.[24–26] After immersion in SBF for 2, 3 or 4 h at 37°C, the samples were characterized by SEM. Apatite-like deposits were noticeable on ZPAA-2 nanofibrous membranes after 4 h of immersion in SBF, whereas fewer deposits were identified on zein and ZPAA-1 membranes (Figure S2B). These SEM results imply that conjugation of Asp on zein improves the in vitro bioactivity of the resulting ZPAA-2 nanofiber.
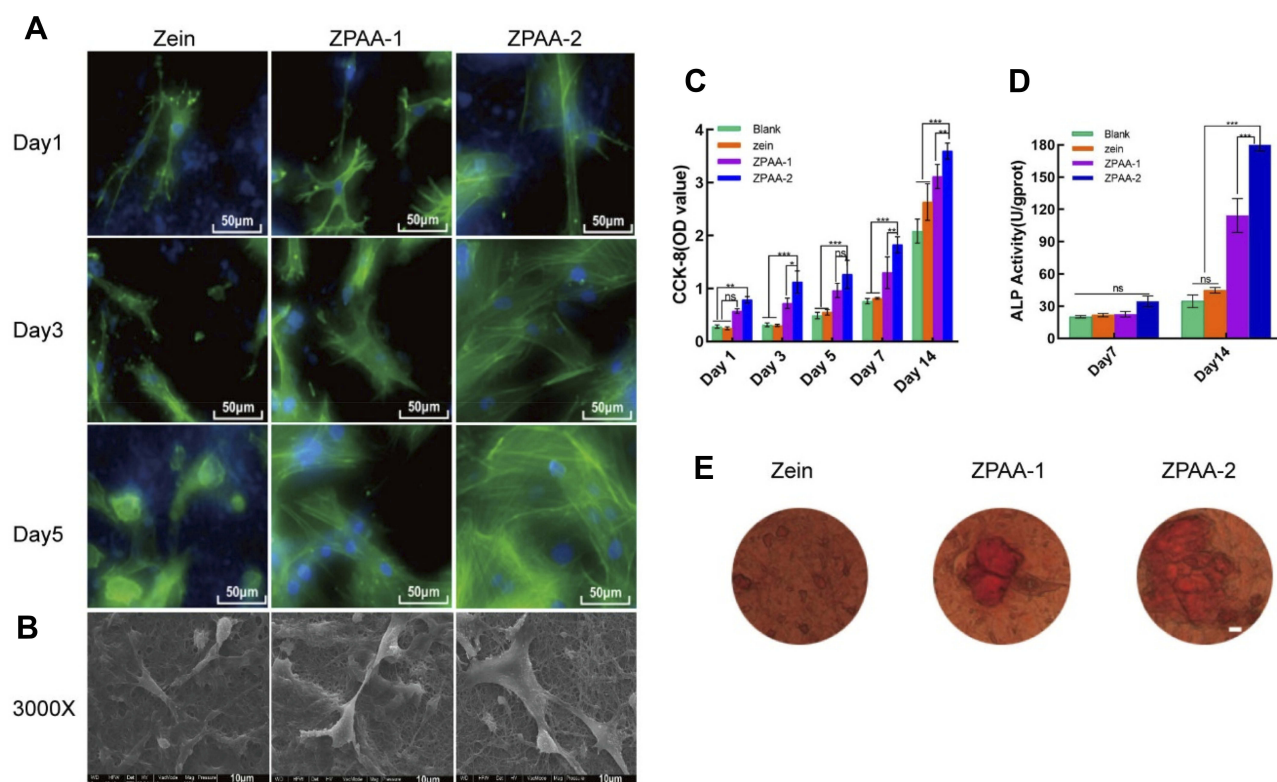
Biocompatibility and Osteogenesis of Zein/ ZPAA-1/ZPAA-2 Nanofibrous Membranes in vitro

Cell Morphology

The morphology of rBMSCs cultured on zein/ZPAA-1/ ZPAA-2 nanofibrous membranes was investigated by both fluorescence staining and SEM. As shown in the fluorescence-staining images (Figure 5A), over the 5-day period rBMSCs spread best on the ZPAA-2 nanofibrous membrane. On the first day, rBMSCs exhibited incomplete spreading over zein/ZPAA-1/ZPAA-2 nanofibrous membranes. After culturing for 5 days, a confluent layer of rBMSCs had become anchored and spread over the ZPAA-2 nanofibrous membrane, generating the largest cell spreading area and the most abundant cytoskeleton. These results show the excellent biocompatibility of the
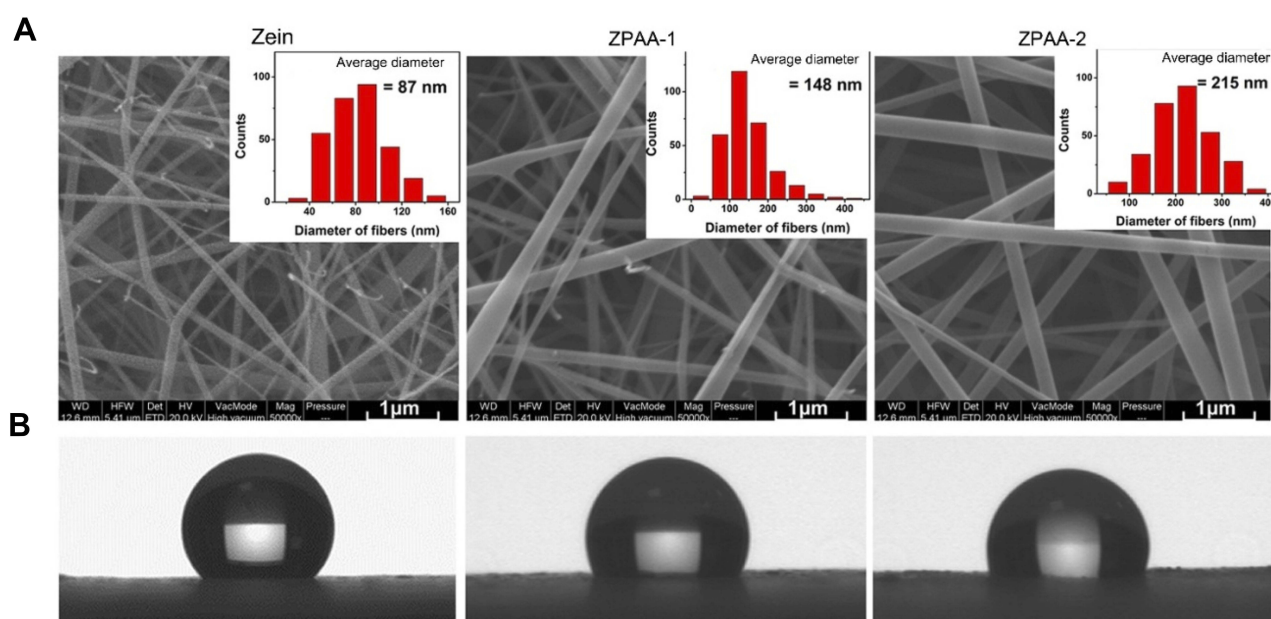
Figure 4 (**A**) SEM images showing the representative morphologies and diameter distributions of zein, ZPAA-1, and ZPAA-2 membranes (**B**) Water contact angles of zein, ZPAA-1, and ZPAA-2 membranes.

Figure 5 Biocompatibility and osteoinductivity of zein/ZPAA-1/ZPAA-2 membranes in vitro. (**A**) Fluorescence microscopy images of the morphology of rBMSCs on zein, ZPAA-1, and ZPAA-2 membranes after culturing for 1, 3, and 5 days. Green indicates the nucleus and blue indicates F-actin. (**B**) SEM images of rBMSCs on zein, ZPAA-1, and ZPAA-2 membranes under a magnification of 3000×, after culturing for 7 days. (**C**) Cell Counting Kit-8 (CCK-8_ assay of rBMSCs viability on zein, ZPAA-1, and ZPAA-2 membranes after culturing for 1, 3, 5, 7 and 14 days (n = 3). (**D**) The relative ALP activities of cells cultured on the membranes (n = 3). (**E**) Alizarin red S staining of cells cultured on the membrane (scale bar = 10 μm). ns > 0.5; *p < 0.05, **p < 0.01, ***P < 0.001.

ZPAA-2 membranes, which appeared to provide an ideal environment for rBMSC growth. After culturing for 7 days, SEM images revealed typical spreading morphologies of rBMSCs on ZPAA nanofibrous membranes, especially in the ZPAA-2 group (Figure 5B). In brief, fully spread rBMSCs with outstretched filopodia extensions were observed on ZPAA-2 membranes, exhibiting polygonal osteoblastic-like cells with obvious filopodia. Overall, ZPAA-2 nanofibers had a superior effect on rBMSC spreading and proliferation than did zein and ZPAA-1 nanofibers.

CCK-8 Assay

The CCK-8 assay was used to evaluate the proliferation of rBMSCs cultured on zein/ZPAA-1/ZPAA-2 nanofibrous membranes for different times. The results showed that in all groups the rBMSCs proliferation increased obviously with time. And the ZPAA-2 group had significantly higher OD values than he blank control/zein/ZPAA-1 group at days 1, 3, 5, 7 and 14 (Figure 5C).

ALP Activity

The osteogenic potential of rBMSCs on zein/ZPAA-1/ZPAA-2 films was measured according to ALP activity; a time-course profile for the three nanofibers is shown in Figure 5D. While there was no difference among the blank control group, zein, ZPAA-1, and ZPAA-2 nanofibers after 7 days of incubation,

the ZPAA-2 nanofiber yielded the highest ALP-enhancing activity of rBMSCs after 14 days of incubation ($p < 0.01$).

ARS

ARS staining was used to evaluate calcium deposition on zein/ZPAA-1/ZPAA-2 films. The images confirm calcium deposition on the ZPAA films, with the ZPAA-2 group showing the greatest calcium deposition (Figure 5E). These results support the finding that Asp inclusion promotes calcium deposition of rBMSCs.

In vivo Bone Regeneration

A critical-size calvarial-defect model (diameter: 6 mm)[27] was developed to assess the bone-forming ability of zein/ZPAA-1/ZPAA-2 films. All rats survived the procedure. Micro-CT images (Figure 6A) showed formation of new bone after the membranes had been implanted for 4 and 8 weeks. The images indicated that at 4 weeks, the defect remained almost void in the blank group, while in the zein group the defect areas were slightly smaller. Moreover, in the ZPAA-2 group the defect was filled with significant new bone at 4 weeks, forming a bone ring sprouting from the edge of the defect. The most conspicuous new bone formation was in the ZPAA-2 group. At 8 weeks, bone repair revealed a similar trend as that observed at 4 weeks; in particular, the bone defect filled with a ZPAA-2
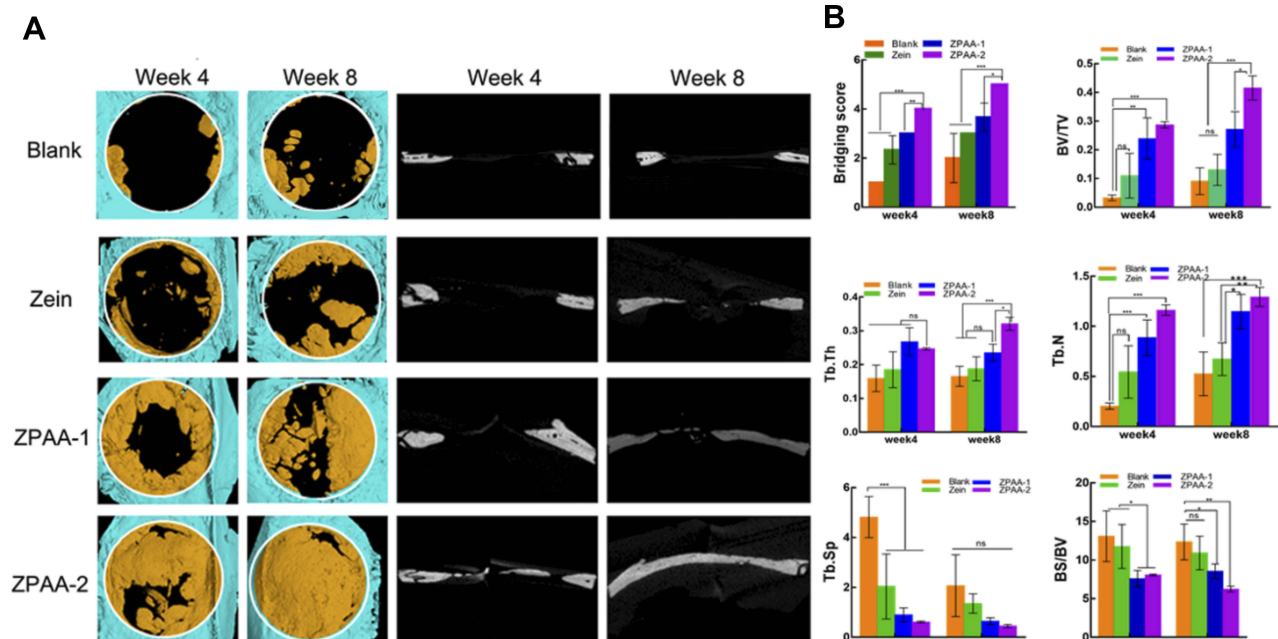
Figure 6 (**A**) Three-dimensional micro-computed tomography-reconstructed images at 4 and 8 weeks postoperatively. (**B**) Quantitative analysis of regenerated bone in terms of the bridging score, bone volume fraction (BV/TV), trabecular thickness (Tb.Th), trabecular number (Tb.N), trabecular separation (Tb.Sp), and bone surface/bone volume (BS/BV). ns > 0.5, *p < 0.05, **p < 0.01, ***P < 0.001.

membrane was almost fully repaired at 8 weeks. The bone repair was further quantitatively evaluated by BV/TV, Tb. Th trabecular separation (Tb.Sp), Tb.N, BS/BV, and bridging values (Figure 6B). The results show that the groups incorporated with Asp (ZPAA-1 and ZPAA-2) had BV/TV, Tb.Th, Tb.N, and bridging values significantly higher than those of the groups without Asp incorporation (blank and zein). Among the Asp-incorporated groups, ZPAA-2 had higher BV/TV, Tb.Th, Tb.N, and bridging values. The Tb. Sp and BS/BV values had the opposite trend.

Bone regeneration in vivo at 4 and 8 weeks was further analyzed by histological staining (Figure 7) and immuno-histochemical staining (Figure 9) to obtain more details. H&E staining (Figure 7A) revealed similar trends to the micro-CT results. At 4 weeks, significant lamellar and woven bone formed in the ZPAA groups, while fibrous tissue filled the area between the trabeculae. In the zein group, obvious undegraded membranes were observed, while lamellar bone was noted in the edge of the defect and a large amount of fibrous tissue was observed between the trabeculae. In the control blank group, a small amount of woven bone and a large amount of fibrous tissue was found. At 8 weeks, the ZPAA-2 group exhibited the most obvious bone healing, and the bone defect was almost fully repaired by well-arranged lamellar bones. In the ZPAA-1 group, a small amount of fibrous tissue was observed in the gap and the lamellar bone was obviously increased compared with that at 4 weeks. In the zein and blank control group, the lamellar bone was also significantly increased compared with that at 4 weeks, and fibrous tissues were observed between the trabeculae. The results showed that new bone formed with time in all four groups, and the process was fastest in the ZPAA-2 group. Moreover, there was no significant difference in the blood vessels for the same group between 4 weeks and 8 weeks, indicating a fairly stable blood supply system in each group. In addition, there was no significant difference in the blood vessels among the four groups at 4 and 8 weeks, which indicated that the blood supply of the bone defect was similar in each group.

Masson staining (Figure 7B) showed the similar trends as H&E staining (Figure 7A). Besides that, in all the groups the red dyed areas were significantly increased from 4 weeks to 8 weeks, and the red dyed area was the most prominent in the ZPAA-2 group. These results showed that the bone matrices in all the groups significantly matured as time progressed, whereas the ZPAA-2 group had the most mature bone matrix. Moreover, the semi-quantitative results

of the Masson staining (Figure 8) revealed that the red dye area in all the four groups showed statistically improvement from 4 weeks to 8 weeks, indicating that the maturity degree of the collagen fibers increased with time. In another word, as time progressed, the maturity degree of the bone matrix was increased. Besides that, the red-stained areas in the ZPAA-1 and ZPAA-2 groups were statistically larger than the zein and blank control groups ($p<0.05$) at 8 weeks, and the area is largest in the ZPAA-2 group. These results revealed that the collagen fibers in the ZPAA-1 and ZPAA-2 groups were more mature than those in the zein and blank control groups, and ZPAA-2 group behave the best. Thus, the maturity degree of the bone matrix was the highest in the ZPAA-2 group.

Bone matrix proteins, such as OCN and Osteocalcin (COL-1) were detected by immunohistochemical staining among all the groups. The results (Figure 9) revealed the similar trends as histological staining. Besides that, the positive staining of OCN and COL-1 indicated non-collagen and collagen matrix formation and deposition in various phase of bone regeneration. And newly formed blood vessels could be seen at both 4 and 8 weeks after implantation, which might enhance the bone formation.

Discussion

Given that self-healing is impossible when a bone defect exceeds a critical size, development of an ideal biomaterial that promotes bone healing is necessary. Zein has been considered a good candidate due to its amphiphilic nature, biocompatibility, nontoxicity and favorable biodegradability, which degraded completely in vivo within 8 months. Moreover, As a plant-derived protein, zein offers superior bio-stability and less possibility to transmit zoonotic disease compared with animal proteins, such as silk fibroin and collagen.[23] Furthermore, zein enhances cell viability, attachment, and proliferation,[28] because of the functional groups in amino acid side chains, which could act as cells recognition sites for attachment.[29] However, its ability to stimulate cell proliferation needs to be improved.[4,30] To achieve this, we focused on Asp, which is the carbon terminal of Arg-Gly-Asp (RGD), and on interactions with bone, both in vitro and in vivo.[31]

The RGD sequence is widely present in cell adhesion proteins and participates in multiple cell-fate decisions.[12,32] As cell-responsive ligands, RGD has become a gold standard in biomaterial modification designs.[28] Li et al[31] modified poly(dimethyl-siloxane) with RGD to improve the adhesion, proliferation, and collagen secretion of
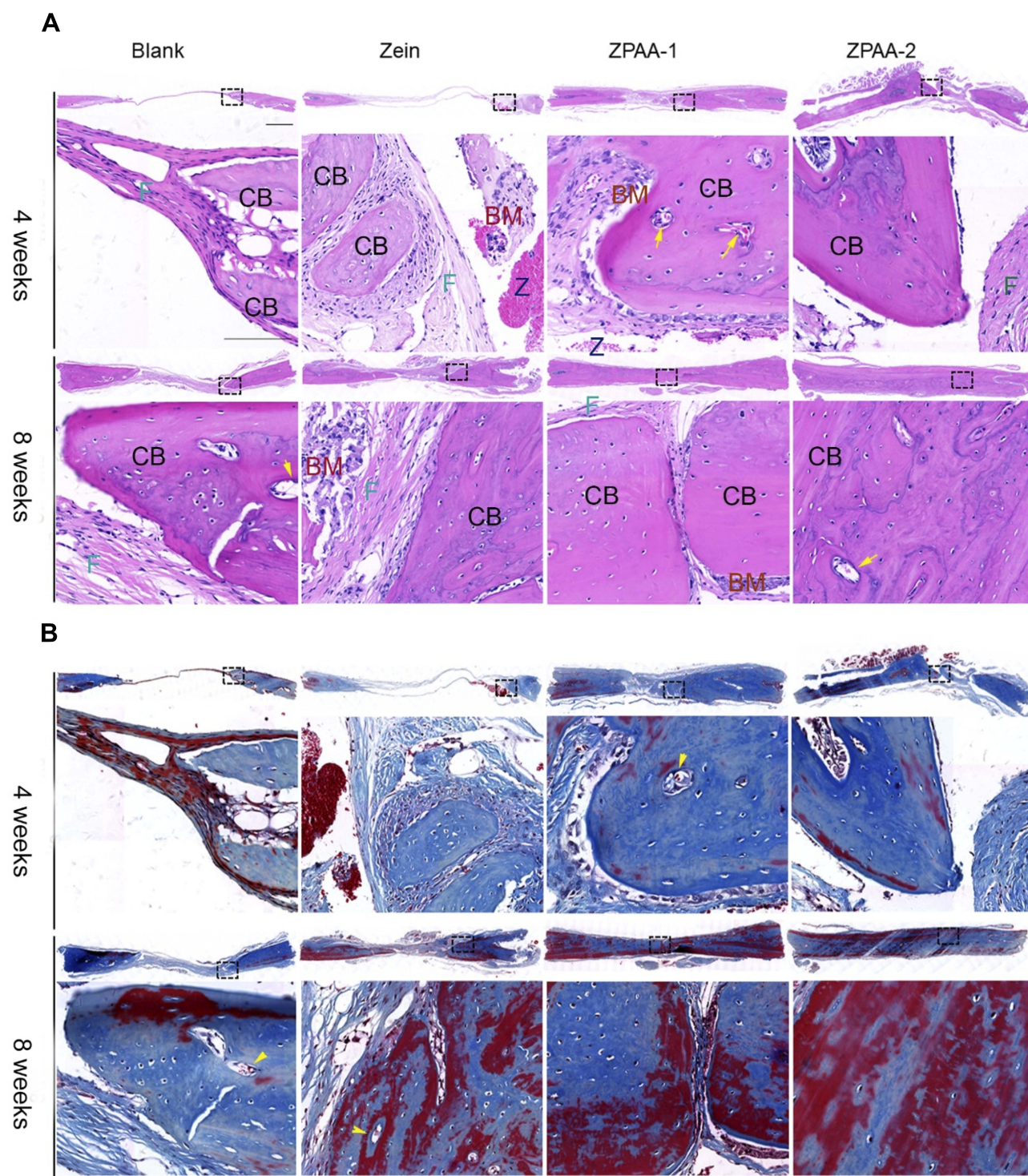
Figure 7 Histological evaluation of bone regeneration in rat calvarial defects at 4 and 8 weeks postoperatively: (**A**) hematoxylin and eosin staining; (**B**) Masson's trichrome staining. CB indicates cortical bone, F indicates fibrous tissue, BM indicates bone marrow, Z represents the location of residual zein/ZPAA materials, and yellow arrows represent vessels (1× and 40× magnification, scale bar = 100 μm).

fibroblasts. As a kind of carboxylic acid, Asp is likely to be the natural bone-targeting ligand in RGD,[31] and it is involved in protein adsorption, MSC/osteoblast attachment, spreading, and proliferation.[8,33–35] In this study, we

developed PAsp-modified zein using click chemistry, which produces stable products by rapid reaction under mild conditions.[3] PAsp-modified zein nanofibrous membranes were prepared using an electrospinning technique
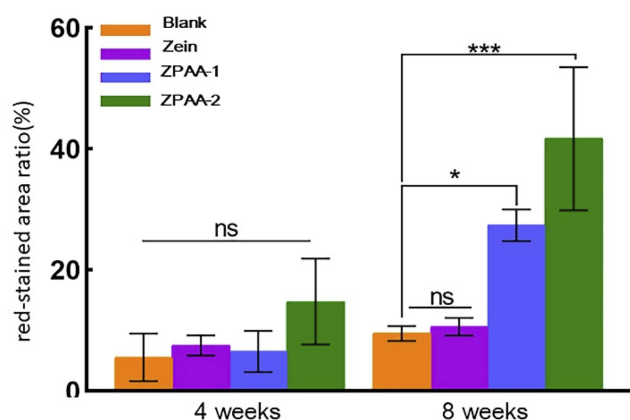
Figure 8 Semiquantitative results of red-stained area ratio based on Masson staining. ns > 0.5, *p < 0.05, ***P < 0.001.

to create nanoscale fibrous membranes with interconnecting pores that mimicked the native structure of ECM.[36]

Zein is a hydrophobic material; improved surface hydrophilicity is necessary for cell adherence and growth.[37] Due to the hydrophilicity of Asp chains, the water contact angles of zein (0% PAsp), ZPAA-1 (5.32% PAsp), and ZPAA-2 (7.63% PAsp) membranes decreased. As revealed by the above results, incorporation of Asp modified the surface morphology of the zein films and enhanced their hydrophilicity, ultimately improving their cytocompatibility.[3] Biomineralization is used to assess whether a biomaterial is ideal for bone tissue bonding and formation; the in vitro hydroxyapatite formation ability reportedly reflects in vivo bioactivity.[23,38] In this study, biomineralization was promoted in ZPAA-2 groups. In another study, Chu et al[39] demonstrated that Asp promotes hydroxyapatite crystallization from the precursor crystal. This phenomenon can be explained by the electronegative carboxy groups of Asp, which provide Ca^{2+}-binding sites and promote the growth of hydroxyapatite.[9] Given that hydroxyapatite is important in bone regeneration, it is reasonable to expect ZPAA-2 nanofibrous membrane to be a promising material for BTE applications.

A biomaterial scaffold for bone regeneration should support adhesion, spreading, proliferation, and osteogenic differentiation of MSCs. In this study, membrane bioactivity was tested by seeding rBMSCs on membrane surfaces. In Figure 5A, the low density and unstretched morphogenesis of rBMSCs on day 1 can be attributed to cell attachment followed by cell growth. However, rBMSCs showed better cell adhesion to the ZPAA-2 membrane than to the zein and ZPAA-1 membranes. The attachment of rBMSCs to the ZPAA-2 membrane increased survival time and cell

viability. Cell attachment is the first stage, followed by cell spreading and proliferation;[40] it typically occurs during the early stage of regeneration and is necessary for establishing layers of cells for matrix maturation. Figure 5A and B demonstrate that rBMSCs seeded on ZPAA-1 and ZPAA-2 membranes spread and proliferated better than did those seeded on the zein membrane from day 3 to day 7, with the ZPAA-2 membrane showing the best results; this indicates that immobilized Asp increases rBMSC proliferation in the early stages of the regenerative process, and a higher Asp content improves cell proliferation and growth. The quantitative CCK-8 results shown in Figure 5C for the proliferation of rBMSCs further confirm the above results. Thus, the results emphasize several key factors related to cell proliferation and growth. First, incorporation of Asp enhanced the hydrophilicity of zein membranes, whereas the wettability of the polymer surface is a key factor influencing material–cell interactions and concomitant cell behaviors.[41] Second, osteoblasts preferentially bind to RGD. As the carbon terminal of RGD, Asp is necessary for bone affinity,[42] and is involved in protein adsorption, MSC/osteoblast attachment, spreading, and proliferation.[8]

Osteogenic differentiation occurs after proliferation. A biochemical marker for the early stage of osteogenic differentiation is ALP activity, which is needed for enrichment of inorganic phosphates within the bone formation site.[43] Furthermore, we used ARS staining to analyze the effect of Asp on late-stage osteogenic differentiation of rBMSCs by surveying the calcium deposited from the maturated osteoblasts. On day 7, the difference in ALP activity among the three groups was not statistically significant. However, day 14 marked the maturation of osteoblasts,[43] as signified by higher ALP activity and a greater amount of calcium deposited on ZPAA-2 membranes (Figure 5D). This proves that Asp efficiently promotes osteoblast maturation. Our results are in accordance with a previous study,[7] in which the addition of Asp to a medium containing osteoblasts promoted osteogenic differentiation and mineralization. Additionally, Asp can act as a nucleating agent and influence apatite growth.[8] Itoh et al[44] showed that synthetic Asp6 peptide has a high affinity for hydroxyapatite and enhances the attachment of osteoblastic line cells to hydroxyapatite. Various noncollagenous bone proteins, such as OPN and OCN, have repeating Asp-rich sequences in their structures, which are potential hydroxyapatite-binding sites;[9,45,46] furthermore, extensive Asp-rich regions are common in the proteins involved in mineralizing systems.[47] Although the proteins associated with mineralized tissues
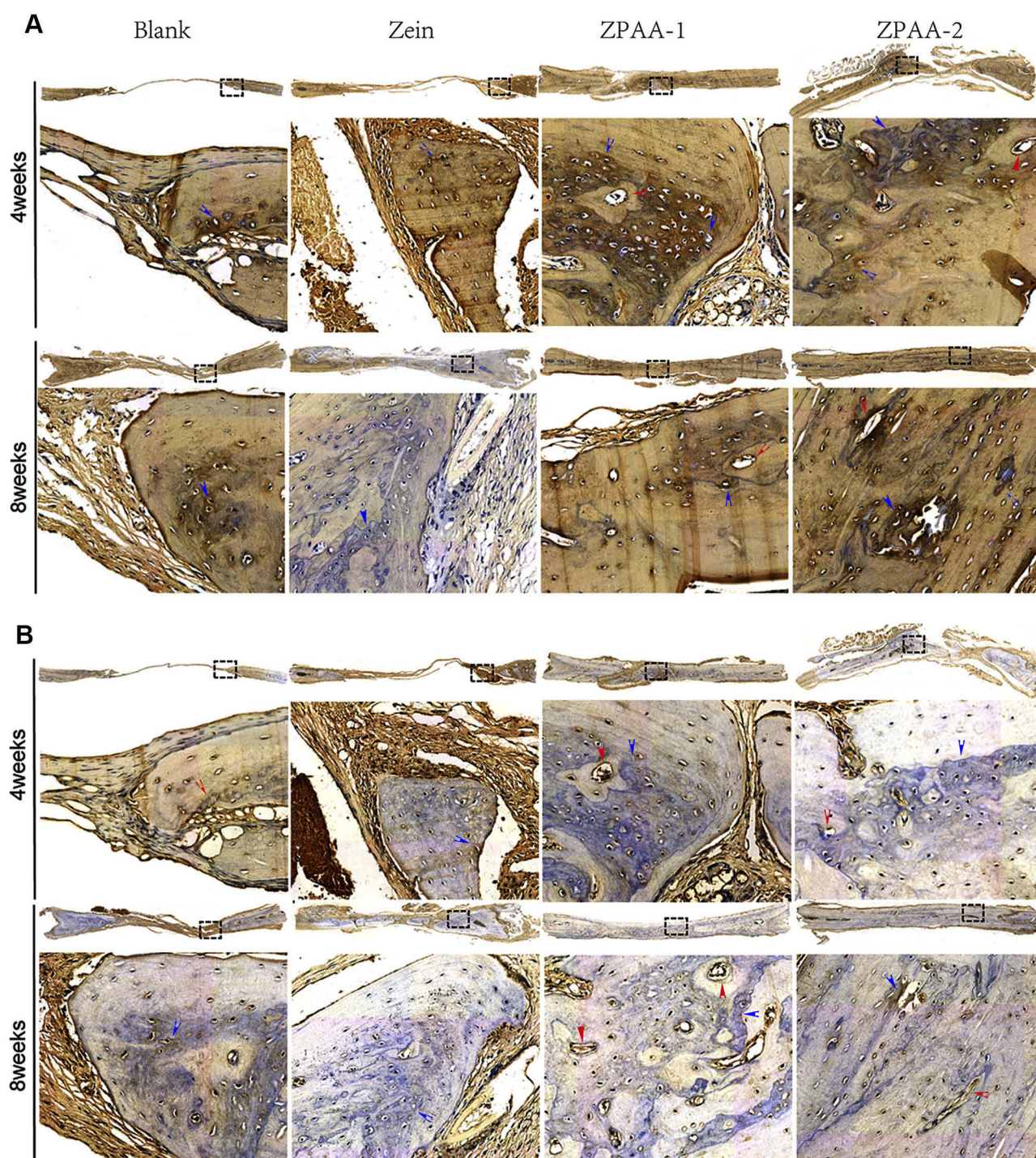
Figure 9 Immunohistochemical evaluations of bone regeneration in rat calvarial defects at 4 and 8 weeks postoperatively: (**A**) collagen type 1 staining and (**B**) osteocalcin staining. Blue arrows represent positive staining, red arrows represent vessels (1× and 40× magnification, scale bar = 100 μm).

vary among species, they are typically rich in Asp.[44] Asp is highly expressed in the small integrin-binding ligand, N-linked glycoproteins (SIBLINGs) protein family, and members of this family play important roles in hydroxyapatite mineralization in the body.[47] Asp can be used as a crystal growth catalyst to modulate biomineralization effectively,[40] and it controls hydroxyapatite mineralization in vivo.[48]

As revealed by Nikolaos et al,[49] biomaterials can be modified with integrin-binding domains to mimic ECM-mediated cell-signaling events. As part of RGD, Asp is an

ideal candidate because it binds to integrin complexes and recognizes various ECM molecules. Asp acts on osteoblastic cells by binding to integrins. One study found that Asp contains peptide sequences, including Asp-Gly-Glu-Ala (DGEA) and RGD, and induces osteogenic differentiation by binding to the α2β1 integrin receptor. In addition, α2β1 is critical in the survival, adhesion, spreading, migration, and differentiation of MSCs.[43] Thus, Asp may also induce osteogenic differentiation by binding to receptor-α2β1. The mechanism of the interaction between HA and Asp is still unclear;[9] however, ionic interactions via the negatively charged Asp sequence and the positively charged calcium within the mineral component of bone are thought to be responsible for the binding effects.[50,51] Palazzo et al[52] suggested that Asp binds Ca^{2+} ions through its −COOH groups. Wu et al[53] revealed that a bone bridge forms between two carboxyl groups from Asp moieties and two adjacent Ca atoms, while the α-NH^{3+} group forms a hydrogen bond with oxygen. Chu et al[39] revealed that Asp plays an important role in optimizing the efficacy of active sites (carboxylate-rich domains) and significantly decreases the interfacial energy barrier, inducing hydrated phase (HP) formation. However, a recent study by Patricia et al[48] revealed that the interactions between ASP and hydroxyapatite are notably mediated by side chains, indicating that both the carboxyl and amine groups contribute significantly to the interaction. Whereas a high content of Asp residues may be effective for collagen binding,[47] incorporation of Asp affects the degree of crystallinity of the apatitic phase, and the crystallinity decreases as the Asp content increases. The presence of Asp helps to control the crystal dimensions and osteogenic differentiation.[8]

The critical-size calvarial defect model (6 mm in diameter in this study) is widely used to assess bone-healing ability in bone repair materials, and the complete healing is still a great challenge.[27] Micro-CT (Figure 6), H&E staining, Masson staining (Figures 7 and 8), and immunohistochemical staining (Figure 9) revealed that ZPAA membranes have the ability to repair critical-sized bone defects effectively. In particular, ZPAA-2 membranes alomst fully repair critical-sized defects with mature bone matrix in 8 weeks, and the stable blood supply of the bone defect might enhance the bone formation. These results imply that Asp incorporation remarkably enhances bone regeneration in vivo; the membrane with an Asp grafting percentage of 7.63% induced superior calvarial bone healing. These results are consistent with in vitro studies and confirm the key role of Asp. Asp has a specific positive effect on bone regeneration in vivo, as it increases the rate of new bone growth; additionally, construction of regenerated bone was superior to that observed in a control group.[7]

All the aforementioned results demonstrate that electrospun PAsp-modified zein is an ideal bone biomaterial. Both zein and Asp are natural materials that are degradable and have no long-term health effects;[54,55] individually, they are good substrates for tissue engineering. A hybrid of these materials can be prepared via a click reaction, which has the advantages of being a mild, effective, robust, safe, environmentally friendly, and nontoxic reaction.[3] As controlling cell behaviors is key to biomaterial development,[12] in this study, we developed electrospun membranes that provide large surface areas for enhancing protein adsorption, as well as a large number of binding sites for cell membrane receptors.[56] Moreover, electrospun membranes form oriented nanofiber webs suitable for engineered tissues, as the webs contribute to cell orientation.[57,58]

Conclusion

In summary, we synthesized chemically modified zein materials with different PAsp contents and demonstrated the feasibility of using electrospun PAsp-modified zein for BTE. ZPAA-2 was shown to be less cytotoxic and more effective in promoting osteogenesis than the other tested materials. Our findings from both in vitro and in vivo studies demonstrate that electrospun PAsp-modified zein can provide a suitable microenvironment for osteogenic differentiation of rBMSCs, as well as for bone regeneration; the optimal membrane appears to have a PAsp grafting percentage of 7.63%. The impact of the nanofibers design regarding the Asp spatial arrangement and density mode on cell−nanofibers interaction would be further investigated to explore the ideal biomaterials in promoting osteogenesis.

Ethics Approval and Informed Consent

The experimental protocol was approved by the Animal Care and Use Committee of Sun Yat-sen University (Permit Number: IACUC-DB-16-0315).

Acknowledgments

Implantology, Guanghua School of Stomatology and the Institute of Polymer Science, Sun Yat-sen University.

Disclosure

The authors report no conflicts of interest in this work.

References

1. Wei T, Dan L, Yuanman Y, et al. Bioinspired trimodal macro/micro/nano-porous scaffolds loading rhBMP-2 for complete regeneration of critical size bone defect. *Acta Biomater*. 2016;32:309–323. doi:10.1016/j.actbio.2015.12.006

2. Yun L, Li-Zhi D, Hai-Peng S, et al. Sustained dual release of placental growth factor-2 and bone morphogenic protein-2 from heparin-based nanocomplexes for direct osteogenesis. *Int J Nanomed*. 2016;11:1147–1158.

3. Yuan Z, Lin Z, Lei Y, et al. "Click" chemistry in polymeric scaffolds: bioactive materials for tissue engineering. *J Controlled Release*. 2018;273:160–179. doi:10.1016/j.jconrel.2018.01.023

4. Jian D, Qingshen S, Jin-Ye W. Basic study of corn protein, zein, as a biomaterial in tissue engineering, surface morphology and biocompatibility. *Biomaterials*. 2004;25:4691–4697. doi:10.1016/j.biomaterials.2003.10.084

5. Lena V, Liliana L, Judith AR, et al. Electrospun Zein Fibers Incorporating Poly (glycerol sebacate) for soft tissue engineering. *Nanomaterials*. 2018;8:150–166. doi:10.3390/nano8030150

6. Laura RA, Alessandro P, Lorena RP, et al. Molecular bionics-engineering biomaterials at the molecular level using biological principles. *Biomaterials*. 2019;192:26–104. doi:10.1016/j.biomaterials.2018.10.044

7. Sara S. Aspartic acid nucleates the apatite crystallites of bone: a hypothesis. *Bone*. 2004;35:108–113. doi:10.1016/j.bone.2004.02.020

8. Elisa B, Paola T, Massimo G, et al. Nanocomposites of hydroxyapatite with aspartic acid and glutamic acid and their interaction with osteoblast-like cells. *Biomaterials*. 2006;27:4428–4433. doi:10.1016/j.biomaterials.2006.04.019

9. Kazuma O, Atsushi I, Kenichiro T, et al. Development of novel radiogallium-labeled bone imaging agents using oligo-aspartic acid peptides as carriers. *PLoS One*. 2013;8:1–9.

10. Brahatheeswaran D, Aby CP, Yutaka N, et al. Biomimetic smart nanocomposite: in vitro biological evaluation of zein electrospun fluorescent nanofiber encapsulated CdS quantum dots. *Biofabrication*. 2012;4:1–14.

11. Ryan JW, Jason AB. Advances in nanofibrous scaffolds for biomedical applications: from electrospinning to self-assembly. *Nano Today*. 2014;9:722–742. doi:10.1016/j.nantod.2014.10.002

12. Lina C, Casey Y, Zijian Z. Functional polymer surfaces for controlling cell behaviors. *Mater Today*. 2018;21:38–59. doi:10.1016/j.mattod.2017.07.002

13. Min SK, Dong HL, Jin J, et al. Topographically defined, biodegradable nanopatterned patches to regulate cell fate and acceleration of bone regeneration. *ACS Appl Mater Interfaces*. 2018;10:1–11.

14. Cai-Yun Z, Wei Z, Li-Bo M, et al. Biomimetic mineralization of zein/calcium phosphate nanocomposite nanofibrous mats for bone tissue scaffolds. *CrystEngComm*. 2014;16:9513–9519. doi:10.1039/C4CE01287A

15. Shixuan C, Ruiquan L, Xiaoran L, et al. Electrospinning: an enabling nanotechnology platform for drug delivery and regenerative medicine. *Adv Drug Deliv Rev*. 2018;132:188–214. doi:10.1016/j.addr.2018.05.001

16. Tas AC, Bhaduri SB. Rapid coating of Ti6Al4V at room temperature with a calcium phosphate solution similar to 10× simulated body fluid. *J Mater Res*. 2004;19:2742–2749. doi:10.1557/JMR.2004.0349

17. Haipeng S, Jinming W, Feilong D, et al. Co-delivery and controlled release of stromal cell-derived factor-1α chemically conjugated on collagen scaffolds enhances bone morphogenetic protein-2-driven osteogenesis in rats. *Mol Med Rep*. 2016;14:737–745. doi:10.3892/mmr.2016.5339

18. Qingqing Y, Jaqueline GLC, Tao X, et al. Three dimensional electrospun PCL/PLA blend nanofibrous scaffolds with significantly improved stem cells osteogenic differentiation and cranial bone formation. *Biomaterials*. 2017;115:115–159.

19. Patrick PS, James DK, Simon Y, et al. Evaluation of bone regeneration using the rat critical size calvarial defect. *Nat Protoc*. 2012;7:1918–1929. doi:10.1038/nprot.2012.113

20. Vo TN, Shah SR, Lu S, et al. Injectable dual-gelling cell-laden composite hydrogels for bone tissue engineering. *Biomaterials*. 2016;83:1–11. doi:10.1016/j.biomaterials.2015.12.026

21. Swee LL, Willie NHT, Chien WO, et al. Rapid swelling and deswelling of semi-interpenetrating network poly(acrylic acid)/poly(aspartic acid) hydrogels prepared by freezing polymerization. *J Appl Polym Sci*. 2016;133:1–9.

22. Csaba N, Benjámin G, Timur A, et al. Poly(aspartic acid) with adjustable pH-dependent solubility. *Acta Biomater*. 2017;49:486–494. doi:10.1016/j.actbio.2016.11.065

23. Masataka N, Joon-Sik P, Woo-Dong J, et al. Study of the quantitative aminolysis reaction of poly(b-benzyl L-aspartate) (PBLA) as a platform polymer for functionality materials. *React Funct Polym*. 2007;67:1361–1372. doi:10.1016/j.reactfunctpolym.2007.08.009

24. Kokubo T, Kushitani H, Sakka S, et al. Solutions able to reproduce *in vivo* surface-structure changes in bioactive glass-ceramic A-W^3. *J Biomed Mater Res*. 1990;24:721–734. doi:10.1002/jbm.820240607

25. Taek GK, Heungsoo S, Dong WL. Biomimetic Scaffolds for Tissue Engineering. *Adv Funct Mater*. 2012;22:2446–2468. doi:10.1002/adfm.201103083

26. Min SK, Joong-Hyun. K, Rajendra KS, et al. Therapeutic-designed electrospun bone scaffolds: mesoporous bioactive nanocarriers in hollow fiber composites to sequentially deliver dual growth factors. *Acta Biomater*. 2015;16:103–116. doi:10.1016/j.actbio.2014.12.028

27. Mikaël MM, Priscilla SB, Esra G, et al. Growth Factors engineered for super-affinity to the extracellular matrix enhance tissue healing. *Science*. 2014;343:885–888. doi:10.1126/science.1247663

28. Shengju G, Huajie W, Qingshen S, et al. Mechanical properties and *in vitro* biocompatibility of porous zein scaffolds. *Biomaterials*. 2006;27:3793–3799. doi:10.1016/j.biomaterials.2006.02.019

29. Linzhi L, Xiang W, Hang L, et al. Zein Increases the cytoaffinity and biodegradability of scaffolds 3D-printed with zein and poly(ε-caprolactone) composite ink. *ACS Appl Mater Interfaces*. 2018;10:18551–18559. doi:10.1021/acsami.8b04344

30. Min H, Huiyi J, Rui W, et al. Fabrication of metronidazole loaded poly (e-caprolactone)/zein core/shell nanofiber membranes via coaxial electrospinning for guided tissue regeneration. *J Colloid Interface Sci*. 2017;490:270–278. doi:10.1016/j.jcis.2016.11.062

31. Kazunori S, Benjamin BR, David AH, et al. Enhanced repair of meniscal hoop structure injuries using an aligned electrospun nanofibrous scaffold combined with a mesenchymal stem cell-derived tissue engineered construct. *Biomaterials*. 2018;154:74–90. doi:10.1016/j.biomaterials.2017.10.053

32. Fa-Ming C, Xiaohua L. Advancing biomaterials of human origin for tissue engineering. *Prog Polym Sci*. 2016;53:86–168. doi:10.1016/j.progpolymsci.2015.02.004

33. Coline P, Said J, Pierre ES, et al. Bioactive peptides grafted silicone dressings: a simple and specific method. *Mater Today Chem*. 2017;4:73–83. doi:10.1016/j.mtchem.2017.02.007

34. Wing-Hin L, Ching-Yee L, Ramin R. A review of chemical surface modification of bioceramics: effects on protein adsorption and cellular response. *Colloids Surf B*. 2014;122:823–834. doi:10.1016/j.colsurfb.2014.07.029

35. Ya-nan G, Xiong L, Hong-ping Z, et al. dft study of the adsorption of aspartic acid on pure, N-doped, and Ca-Doped Rutile (110) surfaces. *J Phys Chem C*. 2011;115:18572–18581. doi:10.1021/jp200598t

36. Jun I, Han H, Edwards J, et al. Electrospun fibrous scaffolds for tissue engineering: viewpoints on architecture and fabrication. *Int J Mol Sci*. 2018;19:744–751. doi:10.3390/ijms19030745

37. Zuwei M, Zhengwei M, Changyou G. Surface modification and property analysis of biomedical polymers used for tissue engineering. *Colloids Surf B*. 2007;60:137–157. doi:10.1016/j.colsurfb.2007.06.019

38. Tadashi K, Hiroaki T. How useful is SBF in predicting *in vivo* bone bioactivity? *Biomaterials*. 2006;27:2907–2915. doi:10.1016/j.biomaterials.2006.01.017

39. Xiaobin C, Wenge J, Zhisen Z, et al. Unique roles of acidic amino acids in phase transformation of calcium phosphates. *J Phys Chem B*. 2011;115:1151–1157. doi:10.1021/jp106863q

40. Qianmin O, Yingling M, Fanqiao Y, et al. Zein/gelatin/nanohydroxyapatite nanofibrous scaffolds are biocompatible and promote osteogenic differentiation of human periodontal ligament stem cells. *Biomater Sci*. 2019;10:1–11.

41. Natália MA, Iva P, Rui LR, et al. Cell behavior through the design of polymer surfaces. *Small*. 2010;6:2208–2220. doi:10.1002/smll.201000233

42. Shugo Y, Hidemasa K, Nozomi H, et al. Development of PEGylated carboxylic acid-modified polyamidoamine dendrimers as bone-targeting carriers for the treatment of bone diseases. *J Controlled Release*. 2017;262:10–17. doi:10.1016/j.jconrel.2017.07.018

43. Hakan C, Samet K, Hilal UG, et al. Bone-like mineral nucleating peptide nanofibers induce differentiation of human mesenchymal stem cells into mature osteoblasts. *Biomacromolecules*. 2014;15:2407–2418. doi:10.1021/bm500248r

44. Itoh D, Yoneda S, Kuroda S, et al. Enhancement of osteogenesis on hydroxyapatite surface coated with synthetic peptide (EEEEEE EPRGDT) *in vitro*. *J Biomed Mater Res Banner*. 2002;62:292–298. doi:10.1002/(ISSN)1097-4636

45. Shohei K, Ryuichi F, Yoshihiro W, et al. Selective drug delivery system to bone: small peptide (Asp)$_6$ conjugation. *J Bone Miner Res*. 2000;15:936–943. doi:10.1359/jbmr.2000.15.5.936

46. Lu C, Ping-Guo D, Hui-Ren W, et al. Degradation and osteogenic potential of a novel poly(lactic acid)/nano-sized β-tricalcium phosphate scaffold. *Int J Nanomedicine*. 2012;7:5881–5888. doi:10.2147/IJN.S38127

47. Anne G, Arthur V. Phosphorylated proteins and control over apatite nulcleation, crystal growth and inhibition. *Chem Rev*. 2009;108:4670–4693.

48. Patricia C, Thomas W. Impact of side chain polarity on non-stoichiometric nano-hydroxyapatite surface functionalization with amino acids. *Sci Rep*. 2018;8:12700–12711. doi:10.1038/s41598-018-31058-5

49. Nikolaos M, Ana F, Molly SS. Biomaterials for cell transplantation. *Nat Rev Mater*. 2018;3:441–457. doi:10.1038/s41578-018-0057-0

50. Tao J, Xiaohua Y, Erica JC, et al. Poly aspartic acid peptide-linked PLGA based nanoscale particles: potential for bone-targeting drug delivery applications. *Int J Pharm*. 2014;475:547–557. doi:10.1016/j.ijpharm.2014.08.067

51. Hasan U, Niki K, Tiejun G, et al. Bisphosphonate conjugation to proteins as a means to impart bone affinity. *Biotechnol Prog*. 2000;16:258–267. doi:10.1021/bp990154m

52. Barbara P, Dominic W, Michele I, et al. Amino acid synergetic effect on structure, morphology and surface properties of biomimetic apatite nanocrystals. *Acta Biomater*. 2009;5:1241–1252. doi:10.1016/j.actbio.2008.10.024

53. Congmeng W, Kang Z, Xiaoqiang W, et al. Dissolution of the calcite (104) face under specific calcite–aspartic acid interaction as revealed by in situ atomic force microscopy. *Cryst Growth Des*. 2012;12:2594–2601. doi:10.1021/cg300194v

54. Hua-Jie W, Sheng-Ju G, Zhi-Xin L, et al. *In vivo* biocompatibility and mechanical properties of porous zein scaffolds. *Biomaterials*. 2007;28:3952–3964. doi:10.1016/j.biomaterials.2007.05.017

55. Matthew BM, Jeffrey DH, Achim G, et al. Synthesis and in Vitro hydroxyapatite binding of peptides conjugated to calcium-binding moieties. *Biomacromolecules*. 2007;8:2237–2243. doi:10.1021/bm070121s

56. Seema A, Joachim HW, Andreas G. Use of electrospinning technique for biomedical applications. *Polymer*. 2008;49:5603–5621. doi:10.1016/j.polymer.2008.09.014

57. Yang F, Murugan R, Wang S, et al. Electrospinning of nano/micro scale poly(L-lactic acid) aligned fibers and their potential in neural tissue engineering. *Biomaterials*. 2005;26:2603–2610. doi:10.1016/j.biomaterials.2004.06.051

58. Tal D, Brian PT, Daniel SK, et al. nanotechnological strategies for engineering complex tissues. *Nat Nanotechnol*. 2010;6:13–22. doi:10.1038/nnano.2010.246